

Journal of the Royal Society of New Zealand

ISSN: (Print) (Online) Journal homepage: www.tandfonline.com/journals/tnzr20

Optical whispering gallery mode resonators: analysing thermo-optic tuning in a silicon sphere

Farhan Azeem, Muhammad Rehan Chaudhry, Muhammad Sohail Anwar, Haseeb Ahmad Khan, Li Ma & Adnan Daud Khan

To cite this article: Farhan Azeem, Muhammad Rehan Chaudhry, Muhammad Sohail Anwar, Haseeb Ahmad Khan, Li Ma & Adnan Daud Khan (29 Aug 2024): Optical whispering gallery mode resonators: analysing thermo-optic tuning in a silicon sphere, Journal of the Royal Society of New Zealand, DOI: 10.1080/03036758.2024.2395909

To link to this article: https://doi.org/10.1080/03036758.2024.2395909

© 2024 The Author(s). Published by Informa UK Limited, trading as Taylor & Francis Group

Published online: 29 Aug 2024.

Submit your article to this journal

Article views: 892

View related articles

View Crossmark data

Citing articles: 1 View citing articles

Full Terms & Conditions of access and use can be found at
https://www.tandfonline.com/action/journalInformation?journalCode=tnzr20

JOURNAL OF THE ROYAL SOCIETY OF NEW ZEALAND
https://doi.org/10.1080/03036758.2024.2395909

Taylor & Francis
Taylor & Francis Group

RESEARCH ARTICLE

OPEN ACCESS Check for updates

Optical whispering gallery mode resonators: analysing thermo-optic tuning in a silicon sphere

Farhan Azeem [a,b,c], Muhammad Rehan Chaudhry [c,d,e], Muhammad Sohail Anwar[c], Haseeb Ahmad Khan[f], Li Ma[a,b] and Adnan Daud Khan [g]

[a] The Dodd-Walls Centre for Photonic and Quantum Technologies, Dunedin, New Zealand; [b]Department of Physics, University of Otago, Dunedin, New Zealand; [c]Graduate School of Science and Engineering, Koç University, Istanbul, Turkey; [d]Department of Biomedical Engineering, University of Engineering and Technology Lahore, Narowal, Pakistan; [e]Department of Electrical Engineering, University of Engineering and Technology Lahore, Narowal, Pakistan; [f]Department of Electrical Engineering, University of Engineering and Technology, Mardan, Pakistan; [g]US-Pakistan Center for Advanced Studies in Energy, University of Engineering and Technology, Peshawar, Pakistan

ABSTRACT

In this work, we discuss and experimentally investigate the whispering gallery modes (WGMs) in a 500 µm radius silicon sphere. We begin by reviewing the basics of WGM resonators, followed by simulations and experimental results obtained with the aforementioned silicon spherical WGM resonator. The recorded WGM signatures in the transmission and scattering spectra excited, in the near-infrared (near-IR) region, agree well with the simulations. Thermo-optic tuning of these WGMs is achieved by introducing a pump laser in the violet-blue region. Red-shifts in wavelength are observed, which increase with the increase in the pump power. A shift of 0.63 nm is observed at a pump power of 6.32 mW. We also study switching by analysing the transient response of the WGM spectra. The measured WGMs exhibit high quality factors ($Q \sim 10^5$), which along with the aforesaid tunability, demonstrates the potential of spherical silicon resonator as a platform for photonic applications, e.g. sensing and communication. In summary, this work contributes towards the understanding of the fundamental physics of WGMs and provides insights into silicon WGM resonators.

ARTICLE HISTORY
Received 9 January 2024
Accepted 26 July 2024

KEYWORDS
Whispering gallery mode resonator; thermo-optic tuning; silicon spheres; silicon resonator; WGMs

Introduction

This section describes the background, basics, and concepts related to whispering gallery modes (WGMs) and whispering gallery mode resonators (WGMRs). The primary objective of this section is to help readers understand the concepts and experimental data detailed in this manuscript. Additionally, we provide a brief overview of the research performed in Aotearoa New Zealand (NZ) related to WGMRs at the end of this section.

CONTACT Farhan Azeem fazeem13@ku.edu.tr, azefa945@otago.ac.nz

© 2024 The Author(s). Published by Informa UK Limited, trading as Taylor & Francis Group
This is an Open Access article distributed under the terms of the Creative Commons Attribution-NonCommercial-NoDerivatives License (http://creativecommons.org/licenses/by-nc-nd/4.0/), which permits non-commercial re-use, distribution, and reproduction in any medium, provided the original work is properly cited, and is not altered, transformed, or built upon in any way. The terms on which this article has been published allow the posting of the Accepted Manuscript in a repository by the author(s) or with their consent.

The gallery of whispers

The term whispering gallery mode is named after the phenomenon discovered in the circular gallery of St. Paul's cathedral in London. In this phenomenon, whispers can be heard by listeners at any other point within the building, given both whisperer and receiver are near the walls of the spherical structure. Hence, such a structure was termed as *whispering gallery* and the phenomenon that occurs within the *whispering gallery waves*, as coined by John William Strutt (Lord Rayleigh) in 1878 (Rayleigh 1878, 1914). This gallery is shown in Figure 1, it is 32 m in diameter and is located at a height of 30 m above the floor (Righini et al. 2011). Lord Rayleigh conducted experiments at St. Paul's cathedral and published his findings titled *The problem of the whispering gallery* (Rayleigh 1910, 1912, 1914) during 1910–1914. In these manuscripts, Rayleigh explained the solution of this problem, attributing the ability of the listener to hear the whispers around the gallery to the refocusing effect of the curved surface, i.e.the sound is contained and focussed by the gallery itself as it travels around its walls. This realisation allowed Rayleigh to conclude that these WGMs are not only possible in sound waves but also in electromagnetic (EM) waves and can lead to practical applications.

Lord Rayleigh's explanation of the whispering gallery of St. Paul's cathedral led to the inauguration of whispering gallery exhibits in other parts of the world, e.g. in 1938, a whispering gallery exhibit was opened in Chicago by the Museum of Science and Industry and later on another was inaugurated in New York (Righini et al. 2011). Apart from St. Paul's cathedral there are many other buildings that demonstrate the phenomenon of the whispering gallery, most notably the temple of heaven in China, Selimiye mosque in Turkey and Sacred heart cathedral in Aotearoa NZ.

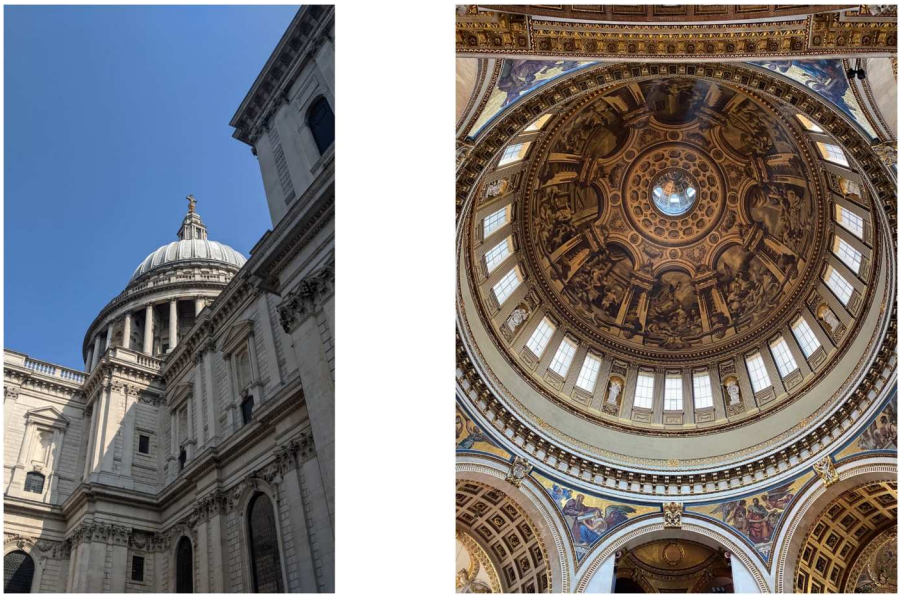


Figure 1. Photographs of the exterior (left) and interior (right) of the dome of Saint Paul's cathedral. The dome shown here was at the heart of Lord Rayleigh's experiments on *The problem of the whispering gallery*. This gallery is also known as the circular gallery and has a diameter of 32 m.

Electromagnetic whispering gallery modes

During the same period when Rayleigh was theorising the existence of WGMs in EM waves, Danish physicist Ludvig Lorenz and German physicist Gustav Mie developed a mathematical solution for the scattering of an electromagnetic plane wave by a homogeneous sphere, known as Lorenz-Mie solution (Lorenz 1890; Mie 1908). A few decades later American physicist Robert Richtmyer analysed the EM modes of a spherical dielectric micro-particle (Richtmyer 1939). In his work, Richtmyer predicted that these spherical particles or resonators can exhibit modes with high quality factors (*Q*-factors) on the order of 10^6. *Q*-factor determines the ability of a resonator to confine light for a period of time and measures a resonator's performance (further elaborated in Section 'Basic parameters for WGMRs'). However, Richtmyer deemed the theoretically predicted *Q*-factor experimentally impossible due to the low quality of optical materials at the time. A more detailed theory was presented by Stratton in his book in 1941 (Stratton 2007).

In 1961, Garrett et al., reported the first observation of lasing using a whispering-gallery-mode resonator (WGMR). This WGMR was based on samarium-doped calcium fluoride (Sm^{2+} doped CaF_2) (Garrett et al. 1961) spheres with diameters between 1 and 2 mm (Lorenz 1890; Mie 1908). Another landmark occasion in the field of WGMRs was the realisation of fused silica resonators by Braginsky et al. (1989). Since then the WGMR has evolved in to a field of its own; with extensive work performed on WGMRs of various structures and high *Q*-factors. The high *Q*-factors are a result of the compact mode volumes of these WGMRs, which lead to high intensity inside them. WGMs are sometimes also referred to as morphology-dependent resonances (MDRs), due to the fact that the modes or resonances in these optical structures are dependent on their geometry or, in other words, their morphology (Lam et al. 1992).

Optical whispering gallery mode resonators

WGMRs are based on round or circular shapes, and light is trapped inside them through total internal reflection (TIR). The confinement of rays via TIR is mainly made possible by the curved boundaries of the resonator. Several circular structures are suitable for WGMs, such as spheres (Chiasera et al. 2010), spheroids (Roselló-Mechó et al. 2019), toroids (Kippenberg et al. 2004), rings (Lambert et al. 2023), discs (Azeem et al. 2021), cylinders (Chantada et al. 2008), among others (Righini et al. 2011). Some of these WGMR shapes currently in use in the Resonant Optics lab Otago and Laser Lab Auckland are shown in Figure 2.

Confinement of light inside WGMRs

As mentioned earlier, light is confined inside the WGMR via TIR, and that is only possible if the ray of light hitting the surface of the WGMR has an angle greater than the critical angle, given by

$$\theta_c = \arcsin \frac{n_{out}}{n_{res}}, \tag{1}$$

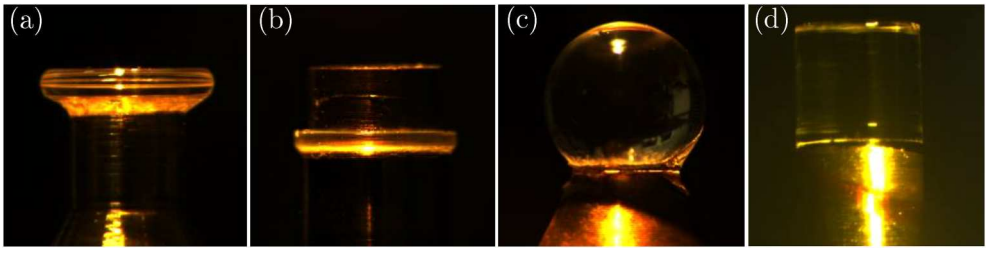


Figure 2. Different geometries of WGMRs. **A,** A disc WGMR attached to a brass rod via mounting wax. **B,** Ring shaped WGMR that is hollow in the centre. A brass rod can be seen going through this hollow centre. **C,** Spherical resonator glued on top of a brass rod. **D,** Shows a cylindrical shaped WGMR. These images were taken at the Resonant Optics laboratory at Otago University, NZ (Ōtākou Whakaihu Waka, Aotearoa).

where n_{out} is the refractive index of the medium surrounding the WGMR, n_{res} is the refractive index of the resonator material and θ_c is the critical angle.

A depiction of TIR via a ray optics picture is shown in Figure 3A. Furthermore, in order for the resonances to take place, the optical path length inside the WGMR must be a multiple integer of the resonator's circumference. Therefore, the resonance condition can be expressed as

$$m\lambda = 2\pi n_{\text{res}} R, \tag{2}$$

where R is the radius of the WGMR, λ is the wavelength of light, and m denotes the integer number of the modes excited by the resonator. This integer number is commonly referred to as the azimuthal mode number, denoted by m.

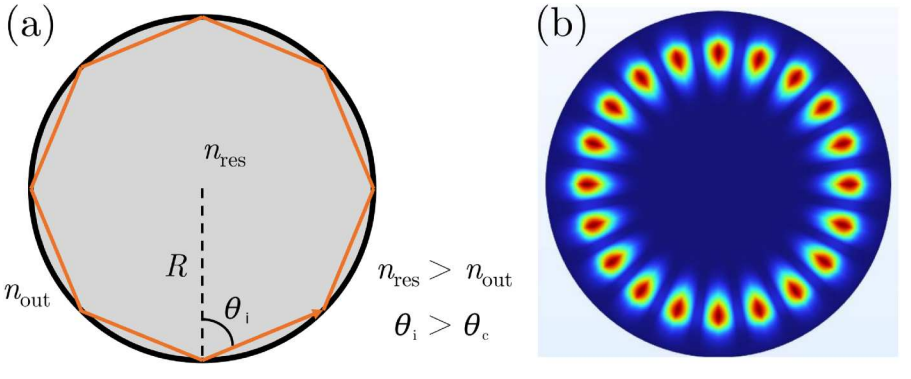


Figure 3. Total internal reflection resulting in confinement of light inside a WGMR. This in turn results in the formation of WGMs. **A,** Shows the two dimensional ray optics picture of trapping of light inside a WGMR. The WGMR has a radius (R) and is composed of a material with a refractive index (n_{res}). The outside medium has a refractive index denoted by n_{out}. The condition for TIR is satisfied when the incidence angle of the incoming light is greater than the critical angle. **B,** Shows the wave optics picture of WGMs inside the resonator depicted in **A**. Here, a WGMR composed of silicon (Si) was simulated in COMSOL. 20 pairs of maxima and minima can be observed in this case denoting the azimuthal number of modes (m).

Coupling mechanisms

Efficient coupling of light to WGMRs is just as important as building a high-Q resonator. In order to effectively couple light to WGMRs, some factors to take into consideration involve the optimal overlap of WGM and coupler mode, critical coupling, selectivity of the mode, efficient phase and mode matched exchange of power (Matsko and Ilchenko 2006; Maleki et al. 2009; Prabhu and Achanta 2020). Some of the widely used coupling techniques include prism coupling (Platt et al. 2024), tapered fibre coupling (Qureshi et al. 2022), free-space coupling (Qian et al. 1986; Zhu et al. 2014), angle-polished fibre coupling (Conti et al. 2011), optical fibre half-coupling (OFHC) (Azeem 2015; Humayun et al. 2018) and waveguide coupling (Cai et al. 2020; Suresh et al. 2023). These methods are depicted in Figure 4.

Free-space coupling or direct illumination is not efficient and is inferior to evanescent coupling due to high losses, which consequently results in lower Q-factors than possible with other methods. This is mainly due to the fact that free-space coupling is achieved by placing nanoscatterers along the boundary of the WGMR or by incorporating engraved gratings (Ballard et al. 2015). Moreover, in free-space coupling, the mode matching of a focussed Gaussian beam is difficult for WGMRs with a larger radius, as the coupling efficiency and Q-factor relies on the wavelength-to-radius ratio (Prabhu and Achanta 2020). On the other hand, in evanescent coupling, the evanescent field from a single input mode is overlapped with the approximately exponentially decaying evanescent field leaking from the WGMR. Evanescent coupling can be performed via a prism, waveguide or a tapered fibre (Righini et al. 2011). Some of the aforementioned coupling techniques are shown in an actual lab environment in Figure 5.

Basic parameters for WGMRs

The quality factor (Q-factor or Q) of a resonator can be expressed by the following equation:

$$Q = 2\pi \frac{\text{Storedenergy}}{\text{Energy loss per cycle}} = \omega\tau, \tag{3}$$

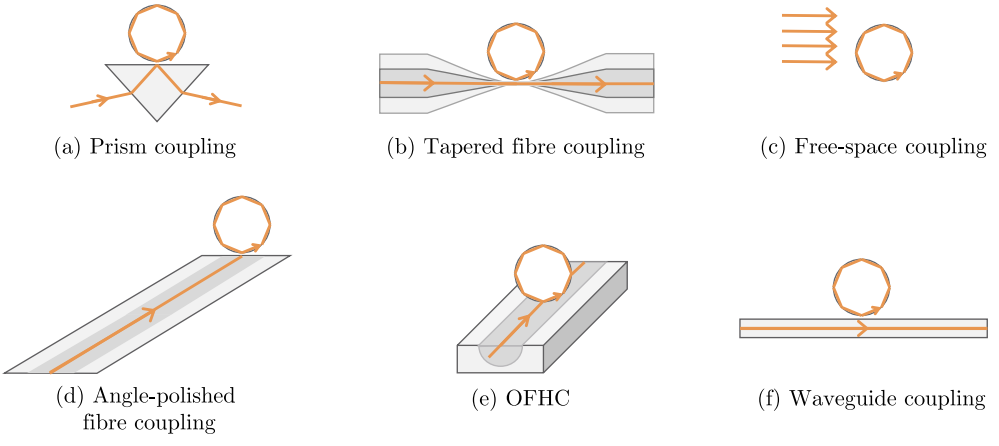


Figure 4. Various coupling mechanisms employed to trap light inside WGMRs via TIR.

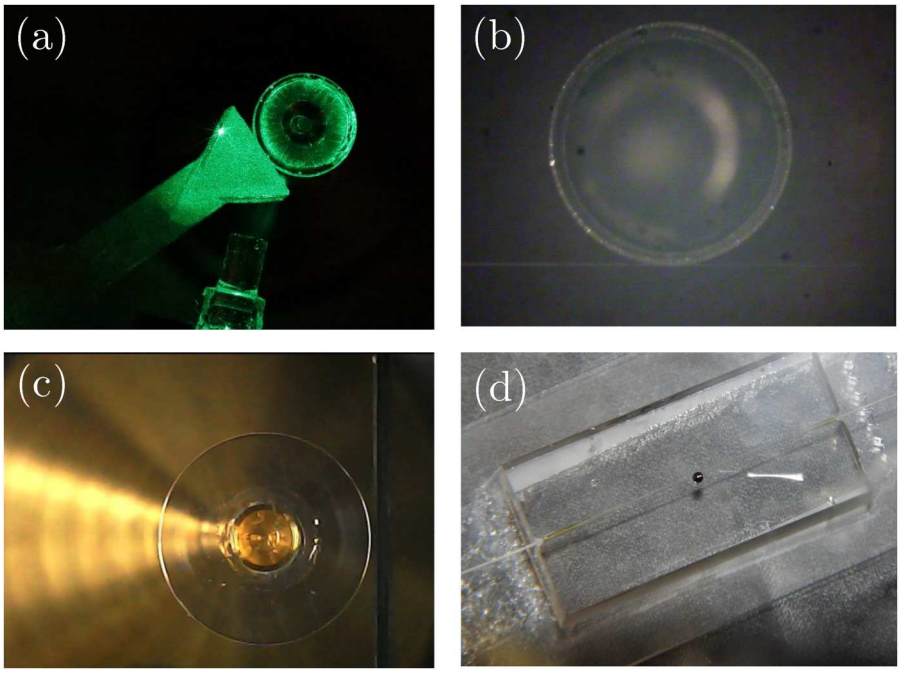


Figure 5. Coupling techniques practically employed in experiments in laboratory setting. **A,** In this scenario a yttrium orthovanadate prism is used to evanescently couple green light into a disc shaped titanium doped sapphire resonator. **B,** A silica tapered fibre is utilised here to couple light into a magnesium fluoride resonator. **C,** Shows a silicon waveguide next to a lithium niobate WGMR. This kind of a configuration is mainly used for terahertz (THz) coupling. **D,** Here, a silicon sphere is placed on an OFHC to excite WGMs. Such a scenario leads to low coupling contrasts due to the high refractive index difference between the WGMR and the coupler.

where ω represents the angular frequency of the resonance mode and τ is the characteristic time associated with the decay of energy in the resonant system. The Q-factor gives a measure of the resolving power of an optical resonator and can be expressed by the number of oscillations underwent by the field before it leaks out of the resonator. The Q-factor given in Equation (3) can also be expressed as

$$Q = \frac{\lambda}{\Delta\lambda}, \tag{4}$$

where λ is the wavelength of the resonant mode and $\Delta\lambda$ is the full width at half maximum (FWHM) of that particular mode at the resonant wavelength (λ). Furthermore, a cavity with higher transmission is able to confine the light for longer intervals of time, which leads to longer constructive interference and results in sharper modes with smaller FWHM, which in turn translates into higher Q-factor values.

The free spectral range (FSR) can be defined as the spectral mode spacing between two WGMs of the same radial mode order q and consecutive azimuthal mode number m. The FSR of disc- and ring-shaped WGMRs is given by

$$\mathrm{FSR} = \frac{\lambda^2}{2\pi n R}, \tag{5}$$

where n in the refractive index and R the radius of the WGMR. However, the FSR of spherical resonators is given by Chýlek (1990)

$$\mathrm{FSR} = \frac{\lambda^2}{2\pi R} \frac{\arctan\sqrt{n^2-1}}{\sqrt{n^2-1}}. \tag{6}$$

Another important parameter for an optical resonator is the finesse ($\mathcal{F}$) of the cavity, given by the following equation

$$\mathcal{F} = \frac{\mathrm{FSR}}{\Delta\lambda}. \tag{7}$$

The higher the $\mathcal{F}$ or Q of the cavity, the narrower are the resonances excited by the cavity. $\mathcal{F}$ gives a measure of the amount of round-trips the confined light can undergo before exiting the cavity. Finesse is an important parameter when it comes to enhancing non-linearity or gain inside the medium of a WGMR (Strekalov et al. 2016).

The total Q-factor of a WGMR is affected by two main types of losses, the internal and the external. Therefore, the total losses inside the WGMR can be expressed as

$$Q_{\mathrm{total}}^{-1} = Q_{\mathrm{internal}}^{-1} + Q_{\mathrm{external}}^{-1}, \tag{8}$$

where Q_{internal} are the intrinsic losses and Q_{external} are the external losses mainly caused by in-coupling or out-coupling mechanisms. Thus, Equation (8) can be re-written as

$$Q_{\mathrm{total}}^{-1} = Q_{\mathrm{int}}^{-1} + Q_{\mathrm{coupling}}^{-1}, \tag{9}$$

where Q_{int} denotes the intrinsic Q-factor of the WGMR and Q_{coupling} shows the losses caused by a coupler, such as the ones shown in Figure 5. Q_{int} is affected by the following losses inside the WGMR (Gorodetsky et al. 1996)

$$Q_{\mathrm{int}}^{-1} = Q_{\mathrm{rad}}^{-1} + Q_{\mathrm{scat}}^{-1} + Q_{\mathrm{abs}}^{-1}, \tag{10}$$

where Q_{rad} indicates the radiation losses, Q_{scat} the scattering losses depending on the surface quality of the WGMR and Q_{abs} the absorption losses of the resonator material. In general Equation (9) can be expressed as:

$$Q_{\mathrm{total}}^{-1} = \Sigma Q_{\mathrm{x}}^{-1}, \tag{11}$$

where Q_{x} shows the losses due to different factors.

The theoretical lower bound of Q-factor can be estimated using Equation (9). The distance between the coupler and the WGMR can lead to three main coupling regimes: over coupling, critical coupling and intrinsic coupling (Sedlmeir 2016; Azeem 2022; Azeem et al. 2022a). In the over-coupled regime the coupler and the WGMR are either in contact or almost touching, which results in the losses induced by the coupler dominating Q_{total} which ultimately leads to lower Q-factors. In the critical coupling regime the losses induced by the coupler are equal to the intracavity losses, whereas in intrinsic coupling regime the Q_{int} dominates the overall Q-factor of the resonator as coupling losses are minimal. Therefore, the upper bound of the Q-factor can be estimated from

Q_{int}:

$$Q_{\text{int}} = \frac{2\pi n}{\alpha\lambda}, \tag{12}$$

where α is the absorption coefficient of the material used to fabricate the WGMR. Intrinsic Q-factors exceeding 1×10^{11} have previously been reported (Savchenkov et al. 2007).

WGMR research in New Zealand

Recently, research based on WGMRs has intensified in Aotearoa NZ. Research groups affiliated with the Dodd-Walls Centre for Photonic and Quantum Technologies actively take part in studies based on WGMRs. In the North Island, the Laser Lab in Auckland has extensively performed research on frequency combs (Sayson et al. 2018), cavity solitons (Qureshi et al. 2022) and parametric oscillation (Ng et al. 2023) with WGMRs fabricated from second (Hendry et al. 2020) and third order nonlinear crystalline materials (Sayson et al. 2019). THz Science and Technology group at the University of Auckland has also performed research in the area and have recently shifted their focus towards THz optics with silicon (Si) WGMRs (Vogt et al. 2019), exploring their applications in sensing (Vogt et al. 2020), metrology (Gandhi et al. 2021) and material characterisation (Vogt 2022). A group at Victoria University of Wellington has recently explored lasing in perovskite coated silica WGMRs (Price et al. 2020). Similarly, a group based in Waikato has recently contributed towards a WGMR based sensing study with gold nanorods (Subramanian et al. 2021).

Some of the WGMRs used in the experiments performed by Laser Lab and THz Science group are fabricated in collaboration with the Resonant Optics (RO) Lab at the University of Otago in the South Island. This Lab currently has the only WGMR fabrication facility in NZ, where resonators are fabricated mostly using the single-point diamond turning technique (Azeem 2022). They have successfully fabricated high-Q resonators using materials such as magnesium fluoride (Sayson et al. 2019; Qureshi et al. 2022), calcium fluoride (Sedlmeir 2016; Trainor 2021), lithium niobate (Azeem et al. 2021), silicon (Vogt et al. 2019), gallium arsenide (Suresh et al. 2023), titanium sapphire (Azeem et al. 2022a, 2022b), lithium tantalate, rare-earths such as yttrium orthosilicate (YSO) (Norman et al. 2022), yttrium orthovanadate (Trainor 2021) and yttrium lithium fluoride (Christensen et al. 2022) among others. RO lab has published results with WGMRs in various areas such as harmonic generation (Trainor et al. 2018), lasing (Azeem et al. 2022a), frequency combs (Rueda et al. 2019), dual frequency combs (Lambert et al. 2023), THz (Suresh et al. 2023) etc. Moreover, another group based in Otago, i.e. Otago Quantum Optics group has previously explored WGMs in rare earths, i.e. mainly YSO (McAuslan et al. 2009). They have used YSO to study cavity quantum electrodynamics (McAuslan et al. 2011), microwave frequency up-conversion (Fernandez-Gonzalvo et al. 2015), measuring optical loss (Norman et al. 2022) and detecting magnetic resonance (Ma et al. 2023). Light and Matter group at Otago has also recently used WGMs to couple Rydberg atoms to THz modes.

In the forthcoming section, we will use the background and concepts explained above to first numerically evaluate the WGMs inside a silicon sphere. Following this, we will use the details from both Sections 'Introduction' and 'Optical tuning of WGMs in a silicon sphere' to experimentally investigate the thermo-optical tuning of WGMs in the

aforementioned silicon spherical WGMR. This represents the first experimental demonstration of direct all-optical thermal tuning of WGMs in a spherical silicon WGMR, to the best of our knowledge. The background and methods provided in this manuscript can be used to fine-tune the resonance wavelengths in silicon WGMR experiments and highlight the potential of silicon WGMRs as temperature sensors based on wavelength shifts. Furthermore, the dynamical tuning data provides a basis for exploring silicon spherical WGMRs as thermo-optical switches.

Optical tuning of WGMs in a silicon sphere

In this section, we will discuss the WGMs excited inside a 500 μm radius silicon sphere. The introduction of this section delves into the relevance of silicon in photonics. Afterwards, we will explore WGMs inside the silicon sphere through simulations. This will be followed by a discussion of WGM tuning, focussing on the theory behind thermo-optic tuning of modes in WGMRs.

Silicon photonics

Renowned for its semiconductor characteristics, silicon boasts advantageous attributes, such as a high refractive index and transparency within the telecommunication wavelengths. Its beneficial properties, including affordability, natural abundance and scalability for mass production, make silicon a widely acknowledged material. Moreover, the swift growth of silicon technology and the enduring validity of Moore's Law have solidified silicon's position as a cornerstone in the solid-state industry for over half a century (Mack 2011).

In the realm of microelectronics, silicon has emerged as a highly potent technological platform over recent decades (Barrios and Lipson 2006). This platform underpins intricate microprocessors, expansive memory circuits, and diverse digital and analogue electronic components. The advent of silicon-on-insulator technology (Bruel 1995) has demonstrated the feasibility of integrating photonic functionalities into this platform, paving the way for silicon-based photonic integrated circuits (PICs) (Chaudhry et al. 2020). PICs facilitate the interconnection of various optical components using silicon waveguides (Soref and Lorenzo 1985).

Silicon photonics leverages the compatibility of silicon with existing semiconductor fabrication technologies, enabling the integration of optical and electronic components on a single chip. This integration has led to the creation of compact and cost-effective devices such as modulators (Witzens 2018), detectors (Sadrozinski et al. 2013) and waveguides (Su et al. 2020), which are essential for high-speed data communication and information processing. Furthermore, silicon has also been extensively used to fabricate various components such as couplers (Shitikov et al. 2018; Farnesi et al. 2021), filters (Liu et al. 2021) and resonators (Humayun et al. 2018). Resonators are used to modulate light, an essential control parameter in photonic circuits.

Silicon based WGMRs

Silicon has been frequently employed in the field of WGMRs, both as a primary material and as a secondary or assisting material. Previously, silicon has been used to coat

materials of lower index, such as silica (Beltaos and Meldrum 2007; Bianucci et al. 2009). Silicon nanocrystals have also been used to fill glass hollow fibres to excite WGMs (Rodriguez et al. 2008). A silicon nitride wedge WGMR has been successfully demonstrated on a silicon chip (Ramiro-Manzano et al. 2012). Furthermore, silicon has been used to implement lithium niobate and lithium tantalate WGMRs on photonics chips (Soltani et al. 2016). A whispering-gallery based photodetector has been demonstrated via the germanium-on-silicon platform (Su et al. 2017).

Silicon microspheres have previously been employed to demonstrate optical channel dropping (Yilmaz et al. 2005). Light emission has also been demonstrated in arrays of silicon microdiscs with Q values on the order of 100 (Ghulinyan et al. 2008). Thermo-optical bistability has been demonstrated in silicon based microdisc WGMRs (Ramiro-Manzano et al. 2013). Moreover, THz WGMs have been realised with a high-Q of 1.5×10^4 in silicon spheres (Vogt and Leonhardt 2018). Thermal tuning of THz WGMs has also been demonstrated in these silicon spheres (Vogt et al. 2018). WGMs were demonstrated in silicon nanopillar resonators (Seo et al. 2019). These nanopillar WGMRs exhibited experimental Q-factors ranging between 871 and 1804 at wavelengths ranging between 950 and 1250 nm.

WGMs have previously been excited in silicon nanowires to enhance their near-IR photo-response (Kim et al. 2019), with the nanowires exhibiting Q-factors between 102 and 548 at near-IR wavelengths. Generation of photon pairs has also been demonstrated in an integrated silicon microdisc WGMR at telecom wavelengths (Kumar et al. 2020). The microdiscs exhibited Q-factors on the orders of 10^5. Microwave WGMs have been explored in silicon rods (Bourhill et al. 2019). These rods had diameters exceeding 10 mm and exhibited Q-factors ranging between 5×10^4 and 5×10^5. A Q-factor of 1.2×10^9 was recently measured at 1550 nm in 1.5 mm thick and 2.5 mm diameter silicon disc WGMR (Shitikov et al. 2018). The main reasons for observing such a high Q-factor are low bulk losses, high quality material, optimum surface quality of the WGMR and an efficient coupling mechanism, i.e. a coupling method involving a silicon hemisphere was employed.

WGMs in a silicon sphere

Similar to Figure 3B, which depicts the m mode number, Figure 6 shows rotationally symmetric 2D simulation (Oxborrow 2007) results depicting the radial mode number (q) and polar mode number (p) in a silicon sphere. These simulations were performed via COMSOL Multiphysics using the parameters given in Table 1.

The panels in Figure 6 illustrate the different mode distributions inside the sphere. Now, the question arises how will these WGMs look in an intensity versus wavelength plot. Figure 7 shows the simulated transmission and reflection or scattering intensity plots for the simulated 500 μm radius sphere. Figure 7A shows the FSR of the mode which agrees well with the calculated FSR using Equation (6). Furthermore, there are some modes in Figure 7A that are better coupled than the rest which potentially shows that these modes are closer to the surface of the sphere than the weaker coupled modes as they lie deeper inside the sphere and possess a higher radial mode order.

Previously, Shitikov et al., predicted a Q_{int} value of 10^{11} (Shitikov et al. 2018) for silicon at 1550 nm using Equation (12). Achieving this intrinsic Q-factor value is challenging

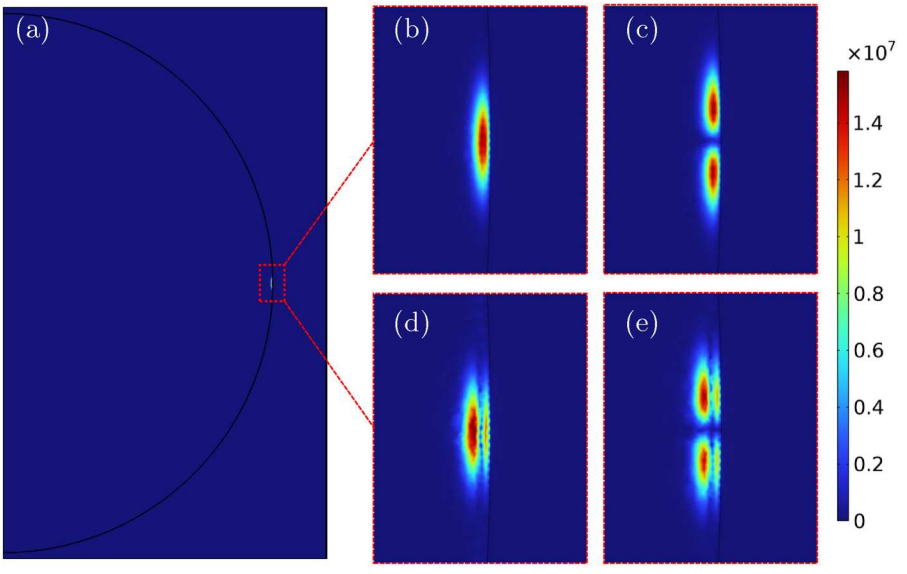


Figure 6. Simulated WGMs inside a silicon sphere of $R = 500$ µm at 1470 nm. **A,** The side view of the silicon spherical resonator at the azimuthal mode number of 7400. Panels **B**–**E,** show the zoomed in images of the area marked by the dashed square showing the mode(s). **B** and **C,** show the cases of polar mode number $p = 0$ and the radial mode number $q = 1$ and $q = 2$, respectively. **D** and **E,** depict the cases of $p = 1$ and $q = 1$ and $q = 2$, respectively.

mainly due to the difficulty in achieving intrinsic coupling. Intrinsic and critical coupling can be realised when an optimal control over the distance between the coupler and WGMR is achieved, which can mainly be performed via prism or tapered fibre coupling (Azeem 2022). The high refractive index of silicon makes utilising both of these methods difficult, i.e. in order to tap into the different coupling regimes, one should employ a high refractive index material prism such as germanium. Furthermore, silicon has extremely low transparency at visible wavelengths which makes coupling light to it via prism coupling technique significantly difficult (Azeem 2022). Moreover, tapered fibres have a significantly lower refractive index than that of silicon which is not ideal to achieve optimal evanescent coupling. The method used by Shitikov et al. (2018) is relatively new as they employ a hemispherical silicon coupler to excite WGMs in their silicon resonator and employ a piezo-electric transducer drive for tuning the distance between the hemispherical coupler and silicon WGMR, which allows them to control the coupler losses and the refractive index of the coupler helps in optimal satisfaction of the TIR conditions. Figure 7B shows the

Table 1. Key parameters used in WGMR COMSOL simulations.

Parameter	Denotation	Value
Radius of the sphere	R	500 µm
Refractive index of the resonator	$n_{silicon}$	3.48
Refractive index of host medium	n_{air}	1
WGM excitation wavelength	λ	1470 nm
Azimuthal mode number	m	7400
Free spectral range	FSR	0.265 nm

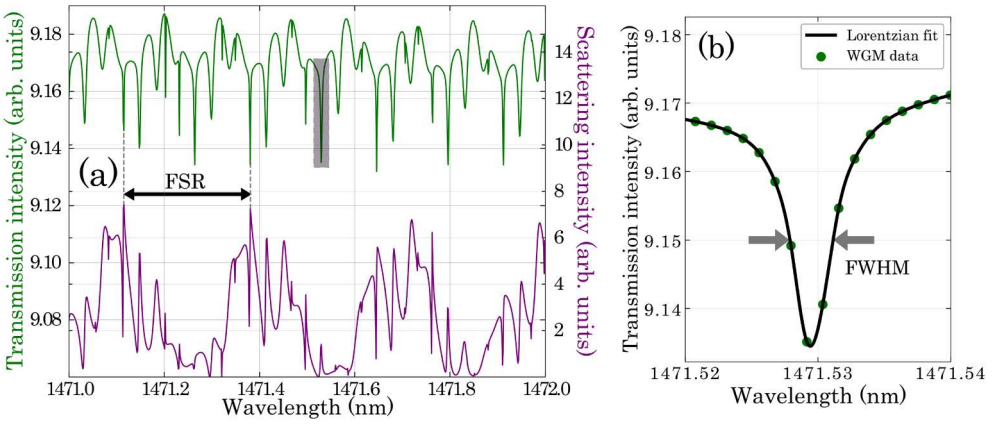


Figure 7. Numerically simulated WGMs showing the free spectral range (FSR) and linewidth of the spherical Si WGMR. **A,** Shows the transmission (shown in green) and scattering (shown in purple) intensities of the WGMR versus wavelength. The predicted FSR from Equation (6) is 0.265 nm. A similar FSR of 0.265 nm can be seen in the plot. **B,** Shows the shaded mode with a central wavelength close to 1471.53 nm shown in **A**. with a Lorentzian fitting applied to accurately extract the FWHM or linewidth ($\Delta\lambda$) of the denoted mode. In this case the $\Delta\lambda = 3.6$ pm, which from Equation (4) translates to a Q-factor of 4×10^5.

predicted $\Delta\lambda = 3.6$ pm determined via using Lorentzian fitting. When this linewidth value is fed to Equation (4) we get a Q-factor value of 4×10^5.

Tuning the central wavelength of WGMs

Tuning the central wavelength of WGMs in optical resonators offers several advantages and applications, e.g. in spectroscopy (von Klitzing et al. 2000), polarisation conversion (Smirnov et al. 2002), three-wave mixing (Breunig 2016) and sensing (Chen et al. 2014; Reynolds et al. 2017). The ability to control the resonance wavelength provides a means to modify the optical properties of these modes for specific purposes. The central wavelength of WGM is either red-shifted or blue-shifted depending on the type of mechanism employed to change the WGM wavelength. A red-shift is achieved when the central wavelength of a mode is shifted towards a longer wavelength (or towards a lower frequency), whereas in a blue-shift the central wavelength is shifted towards a shorter wavelength (or an increase in the central frequency is observed) (Azeem et al. 2021). Figure 8 depicts the red-shift in the central wavelength of WGMs. Black shows the normal spectrum and red shows the same spectrum after the central wavelength of the WGMs is shifted towards longer wavelengths.

Previously, various methods have been employed to tune the central frequency of modes in WGMs, such as electro-optic tuning (Savchenkov et al. 2003; Lin et al. 2022), where electrodes are used to apply electric field across the WGMR to achieve wavelength shifts. Another method is substrate tuning, when substrates of varying refractive indices are brought inside the evanescent field to achieve wavelength shifts (Foreman et al. 2016; Azeem et al. 2021). Furthermore, WGMs can also be tuned by applying pressure (Ioppolo and Ötügen 2007) and strain (Ilchenko et al. 1998). These methods have opened the doors for various sensors based on monitoring the shift in resonance.

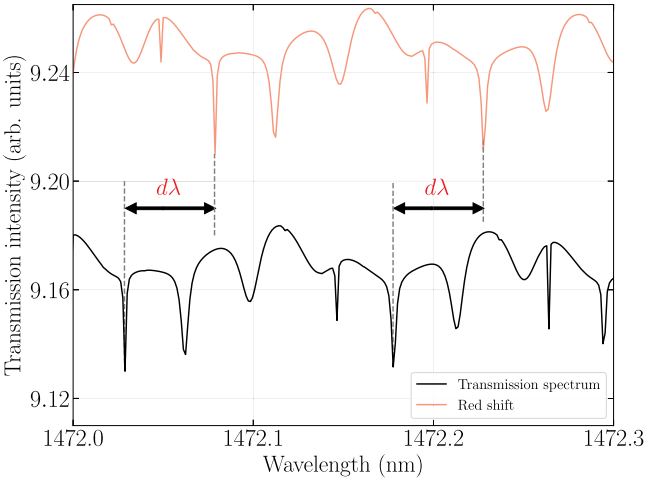


Figure 8. The simulated red-shift in the WGM spectra of the 500 μm silicon sphere when excited at telecom wavelengths.

However, some of these methods usually end up in deforming the WGMR, rendering them unsuitable for certain situations.

Another strategy for achieving wavelength tuning of WGMs is using the thermo-optical tuning (Tapalian et al. 2001; Ward and Chormaic 2010; Vogt et al. 2018). This method involves introducing a source of heat such as a heater to change the temperature of the WGMR material which results in a change in its refractive index, which in turn results in a wavelength shift. However, if too much heat is applied this can also result in the thermal expansion of the WGMR material which can affect the coupling of the modes. The wavelength shifts in WGM spectra realised using this technique have previously been used to achieve accurate temperature sensors using WGMRs (Strekalov et al. 2011). Another strategy used to implement the thermo-optical tuning is by introducing an optical pump (Tewary et al. 2006), where a pump laser operating at wavelengths lying inside the absorption range of the host material is employed to tune the resonances of the excitation laser. This method has previously been used to tune the WGMs of a silicon coated silica sphere by introducing a pump at 488 nm to tune the WGMs excited via a 1450 nm laser. However, both the lasers were introduced via the same tapered fibre employed to couple light into the WGMR. Furthermore, this all-optical technique has also been used to realise thermo-optical tuning of silicon-on-chip ring resonators (Koehler et al. 2018).

In order to perform thermo-optical tuning of WGMs, it is essential to understand the mechanism behind it. The wavelength of a WGM is given by the resonance condition listed in Equation (2):

$$\lambda = \frac{2\pi nR}{m},$$

in order to evaluate the changes in the wavelength of WGMs due to change in temperature, we take the derivative of both sides with respect to temperature (T):

$$\frac{\mathrm{d}\lambda}{\mathrm{d}T} = \frac{2\pi}{m}\left(\frac{\mathrm{d}n}{\mathrm{d}T}R + n\frac{\mathrm{d}R}{\mathrm{d}T}\right),$$

by dividing both sides by $m\lambda$ we get the following expression:

$$\frac{1}{\lambda}\frac{\mathrm{d}\lambda}{\mathrm{d}T} = \frac{1}{R}\frac{\mathrm{d}R}{\mathrm{d}T} + \frac{1}{n}\frac{\mathrm{d}n}{\mathrm{d}T}. \tag{13}$$

A similar approach is taken by He et al. (2018) to determine the correlation between wavelength shifts and temperature. Now, on the right side of Equation (13), we have two terms, which can be denoted by:

$$\alpha = \frac{1}{R}\frac{\mathrm{d}R}{\mathrm{d}T}, \quad \beta = \frac{\mathrm{d}n}{\mathrm{d}T}, \tag{14}$$

where α and β are the thermal expansion and the thermo-optic coefficients, respectively. Therefore, Equation (13) can be rewritten as

$$\frac{1}{\lambda}\frac{\mathrm{d}\lambda}{\mathrm{d}T} = \alpha + \frac{1}{n}\beta. \tag{15}$$

Moreover, the thermal expansion coefficient of silicon has previously been measured at room temperature (Okada and Tokumaru 1984; Watanabe et al. 2004):

$$\alpha = \frac{1}{R}\frac{\mathrm{d}R}{\mathrm{d}T} = 2.6 \times 10^{-6\circ}\mathrm{C}^{-1}. \tag{16}$$

The thermo-optic coefficient of silicon at 1550 nm and close to room temperature is given by Masini et al. (2002), Frey et al. (2006) and Komma et al. (2012)

$$\beta = \frac{\mathrm{d}n}{\mathrm{d}T} = 1.86 \times 10^{-4\circ}\mathrm{C}^{-1}. \tag{17}$$

By using Equations (16) and (17) together with Equation (15), the overall change in temperature of the silicon WGMR can be determined via evaluating the shift in wavelengths. Next, we will experimentally utilise the aforementioned optical pumping method to determine the shift in the silicon WGMs. This will help us in determining the change in temperature as well.

Experimental demonstration of WGM tuning

In this section, we discuss the experiment devised to showcase the optical tuning of the WGMs of a silicon sphere, followed by the results obtained using the aforementioned experimental configuration.

Experimental setup

Experimental configuration assembled to excite and tune WGMs in the silicon WGMR is depicted in Figure 9. At the heart of the setup is the silicon sphere of 500 μm radius. A photograph of this sphere obtained via a scanning electron microscope (SEM) can be seen in Figure 9B. A tunable near-IR laser was used along with an OFHC (previously depicted in Figures 4E and 5D) to excite the WGMs in the sphere. Coupling was achieved by mounting the sphere via a suction syringe and then placing it on the OFHC. This type of method does not give much versatility or coupling control when compared to prism or

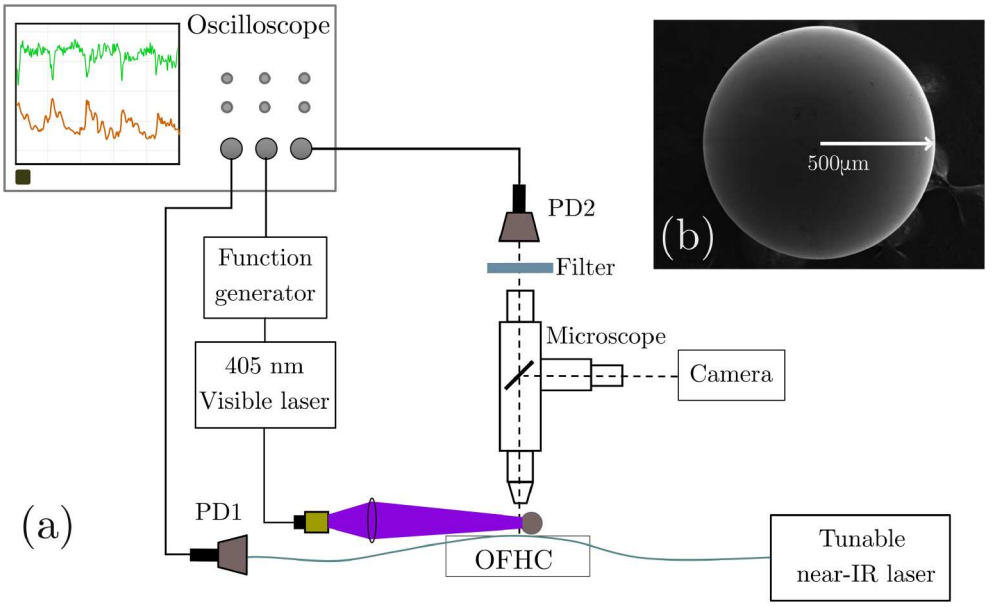


Figure 9. A, Schematic of the experimental configuration. At the core of the experimental setup is the 500 μm radius silicon spherical WGMR. The WGMs are excited in the silicon sphere via a tunable near-IR laser and an OFHC. This method is depicted and photographed in Figures 4E and 5D. **B,** The scanning electron micrograph of the silicon spherical WGMR.

tapered fibre coupling, as there is no mechanism such as a piezo controller to help fine-tune the distance between the coupler and the WGMR in order to access various coupling regimes (Azeem 2022). However, it is a quicker method that can be used to couple to a material that has minimal transparency in the visible wavelength range. Additionally, in this method, the coupling spots on the OFHC can be monitored using a visible laser, such as a red fibre laser, commonly referred to as a visual fault locator (VFL). The main advantage of this method is the reduced time spent finding the coupling spot, which in case of prism coupling, would require an infrared camera. The main disadvantages are the lack of coupling control and efficiency. Next, the output from the OFHC was connected to an InGaAs photodiode (PD). The scattered light from the resonator was collected using a microscope and another InGaAs PD. Both the PDs were connected to an oscilloscope to monitor and record the transmitted and scattered WGMs. The microscope was also used to observe the coupling spots on the OFHC using a camera. Furthermore, a violet pump laser (λ = 405 nm) was focussed on the silicon microsphere to thermo-optically tune the WGMs excited by the telecom laser. This pump laser was connected to a function generator to operate in pulsed mode to control its output power. The excitation laser was operated at a power of less than 1 mW, which is significantly lower in magnitude when compared to the higher pump powers used in the experiment.

Results and discussion

Figure 10A shows the recorded transmission spectra, while Figure 10B shows the scattering spectra of the silicon WGMR excited by the near-IR laser. In Figure 10, the WGM

spectra that were recorded when the violet pump laser was off, are shown in black, whereas the spectra recorded when the pump laser was on, are shown in red. The pump laser was operated at an average power of 6.32 mW at 80% duty cycle and was focussed down to a spot of 170 μm in diameter, corresponding to an average intensity of 28 Wcm^{-2}. The pump laser was driven by an electronic signal generator operating at duty cycles between 20% and 80%. A *Q*-factor on the order of 10^5 was recorded by measuring the linewidth of modes using the Lorentzian fit method shown in Figure 7B and then utilising Equation (4). The narrowest linewidths of the WGMs in Figure 10 are on the order of $\Delta\lambda$ = 0.01 nm, which corresponds to *Q*-factors on the order of 10^5 for the operating wavelength of λ = 1472 nm. However, the intrinsic *Q*-factor values can turn out to be way higher if a mechanism is introduced to minimise the coupling losses by controlling the distance between the coupler and the WGMR (Sedlmeir 2016; Azeem 2022).

The pump power was gradually increased by increasing the duty cycle. It can be seen in Figure 10 that the WGMs keep on moving to longer wavelengths with an increase in the pump power, mainly due to the absorption of the pump in the silicon sphere. This consequently changes the temperature of the sphere, which in turn changes the refractive

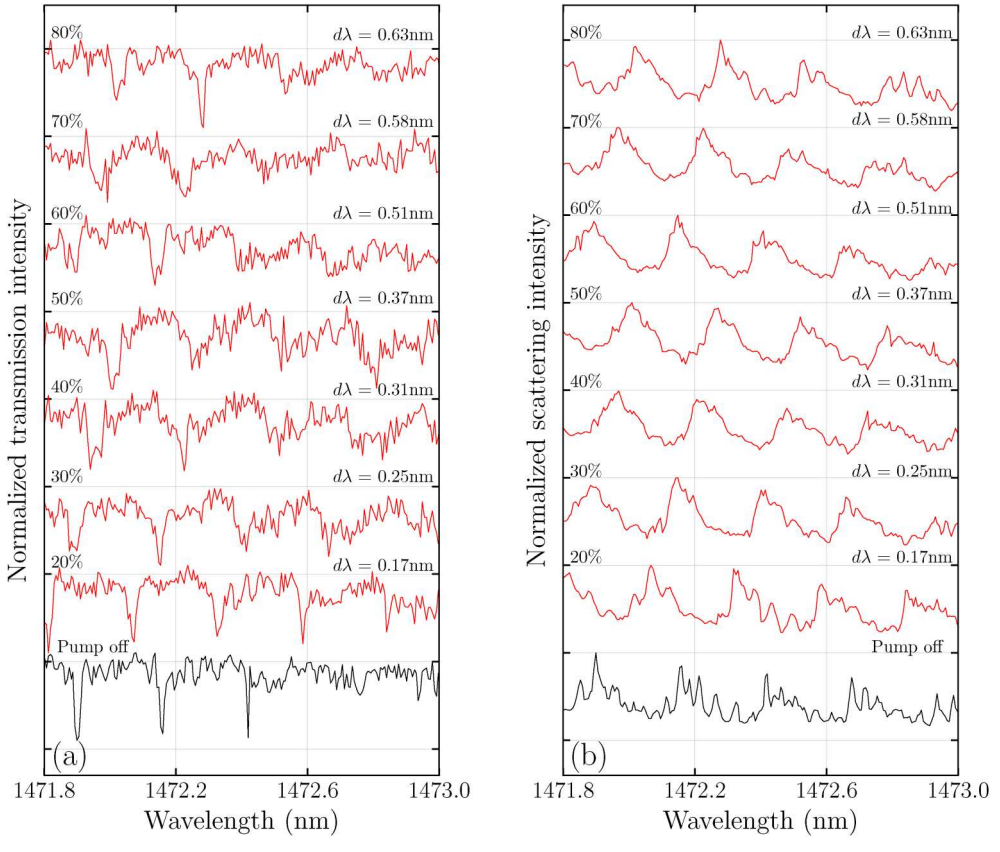


Figure 10. WGM spectra of the silicon WGMR. **A,** Displays the transmission and **B** shows scattering WGM spectra for 0% to 80% duty cycle tuning by the 405 nm wavelength pump laser. The WGMs shift to longer wavelengths with an increase in 405 nm pump laser duty cycle.

index and the radius of the sphere as shown in Equation (15). This ultimately leads to a change of the optical path length of the modes. Since this is a red-shift the modes are getting pushed towards the surface of the WGMR (Vogt et al. 2019; Azeem 2022).

It can be observed in Figure 10 that the spectra are quite populated. This is mainly due to the size and the geometry of the WGMR. Spherical resonators exhibit degeneracy (Kippenberg 2004), therefore a coupling mechanism where the distance between the WGMR and the coupler can be tuned is desirable. Unfortunately, we lacked such a mechanism and relied on placing the spherical WGMR on different coupling points of the OFHC to tackle a highly populated WGM spectrum. Another way to tackle this is by utilising prism coupling method and changing the coupling angle (Norman et al. 2022) or by breaking the spherical symmetry, i.e. by introducing a different radius of curvature, which is why for certain experiments disc and ring shaped WGMRs are preferred (Sedlmeir 2016). Different polarisation modes undergoing variable shifts can be observed in Figure 10A by following the shift in the left most mode of the $d\lambda = 0.17$ nm case, i.e. with the increase in duty cycle, the mode is red-shifting and is getting closer to another mode which is shifting with a different rate. If this mode is observed at 80% duty cycle, it can be seen that it has a better definition now as it has totally crossed the mode undergoing a slower shift (Rueda et al. 2016; Werner et al. 2018; Azeem 2022).

By re-arranging Equation (15) we can calculate the thermal tuning coefficient of silicon ($\mathrm{d}\lambda/\mathrm{d}T$), i.e.

$$\frac{\mathrm{d}\lambda}{\mathrm{d}T} = \lambda\left(\alpha + \frac{1}{n}\beta\right), \tag{18}$$

now by plugging values of Equations (17) and (16) and values of $\lambda = 1472.5$ nm and $n = 3.48$ (Li 1980), we get:

$$\frac{\mathrm{d}\lambda}{\mathrm{d}T} = 0.078\ \mathrm{nm}/^{\circ}\mathrm{C}, \tag{19}$$

this implies that a shift of 1 nm will be induced by a temperature change of 12.65°C. Figure 11 shows the correlation between the pump power, wavelength shift and temperature change. The method presented here can be utilised to measure the heat transfer coefficient (h) of a material with some modifications and by utilising the Newton's law of cooling (Tewary et al. 2006), i.e.

$$h = \frac{P_{\mathrm{abs}}}{A\,\mathrm{d}T}, \tag{20}$$

where h is the heat transfer coefficient, P_{abs} is the absorbed pump power and A is the surface area of the WGMR. However, it is recommended to evanescently couple the pump to the WGMR as well, which will result in the pump being uniformly absorbed by the resonator, as opposed to the current scenario where only a portion of the resonator is illuminated by the pump via free-space illumination.

Additionally, in order to observe the transient thermo-optic response of the silicon microsphere, the pump laser was operated at different repetition rates, while illuminating the silicon WGMR at varying duty cycles. Figure 12 shows the timing plots of the switched scattering for various values of the pump laser duty cycles between 15% and 85% at a repetition rate of 7 Hz, while the wavelength of the excitation laser was kept at

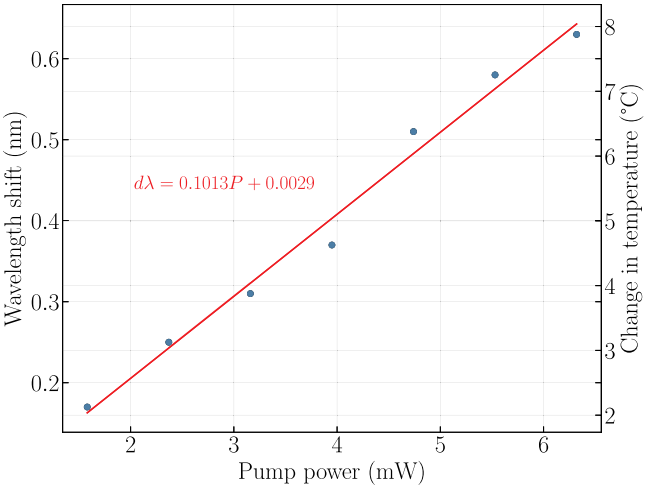


Figure 11. Pump power (*P*) versus shift in wavelength and the corresponding change in temperature. It can be observed that there is an almost linear relationship between the pump power and wavelength shift, which is displayed by the fitting and equation. An increase in the pump results in an increase in the overall temperature of the resonator, consequently causing the red-shifts.

1472.75 nm. The switching pulse on-time of the pump laser is shown by the grey shaded areas. It can be observed in Figure 12 that, during the on-time, a specific change is induced by the pump in the WGM signal which potentially has an effect on the refractive index of silicon WGMR, whereas during the off-time of the pump laser, the refractive index of silicon reverts back to its steady state value. Furthermore,

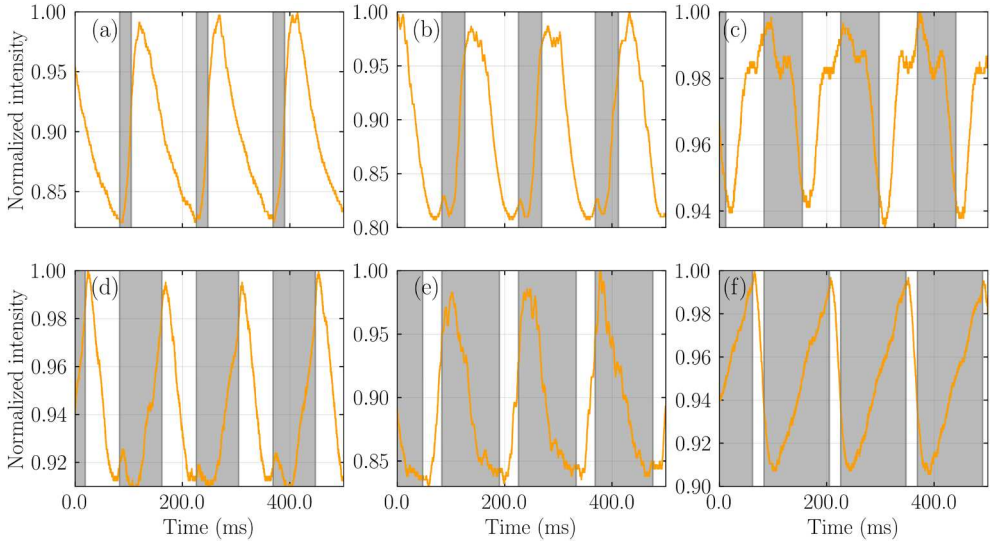


Figure 12. Normalized scattering intensity of the WGM signal versus duty cycle times of the pump laser. Panels **A**–**F,** show the scattering from the sphere recorded via an InGaAs photodiode at duty cycles of 15%, 30%, 50%, 55%, 75% and 85% respectively. The shaded area in the plots denote the on-time of the pump laser, whereas the white area denotes the pump off-time.

there are synchronous patterns in the resonance spectra, which repeat throughout the on-time and the off-time of the pump laser pulse and are opposite in nature to each other.

Conclusion

In this manuscript we discussed the background of WGM resonators along with a brief commentary on the research undertaken in Aotearoa NZ on WGMRs. Furthermore, we used a spherical silicon WGMR as an archetype to explain the mechanism behind WGMs using simulations. Afterwards, we utilised this as a basis to explain an all-optical tuning experiment performed on a silicon sphere of 1 mm diameter. In summary, the WGMs of a silicon sphere excited via a near-IR laser were tuned by introducing a pump laser operating at a wavelength of 405 nm, which lies inside the absorption region of silicon. The WGMs exhibited Q-factors on the order of 10^5 and FSR of $\Delta\lambda = 0.26$ nm, which correlate well with the estimated values. A maximum red-shift of 0.63 nm was observed at an average pump power of 6.32 mW and dynamic tuning of the WGMs was observed during the on- and off-times of the pump laser.

The versatility of WGMRs is underscored by their sensitivity to external factors, including temperature, pressure and refractive index changes, making them tunable and ideal for high-performance sensors. This tunability provides a means for dynamic control and modulation of the WGM resonance, which can potentially aid in manufacturing re-configurable photonic devices. This is particularly useful in applications such as tunable filters, switches and modulators. Moreover, the methods listed here can be used as a basis to realise a silicon WGMR based temperature sensor, or to determine the heat transfer coefficient of silicon. Finally, by implementing such a resonance tuning mechanism the phase-matching conditions can be satisfied in WGMRs fabricated from materials possessing high absorption in the visible wavelength range such as silicon nitride and germanium.

Acknowledgments

F.A, M.R.C and M.S.A Would like to acknowledge the support of Higher Education Commission of Pakistan. F.A would also like to acknowledge discussions with Ali Serpengüzel. We are also thankful to Katy Collins and Carlton Reeve for providing the images of exterior and interior of St. Paul's cathedral, respectively. F.A would like to thank Assoc. Prof. Dr. Harald Schwefel for his guidance and for approving University of Otago postgraduate writing bursary, which aided in the writing and finalising of this article. F.A would like to thank Mallika Irene Suresh for providing the photograph of waveguide coupling to WGMR.

Disclosure statement

No potential conflict of interest was reported by the author(s).

ORCID

Farhan Azeem http://orcid.org/0000-0001-7216-7035
Muhammad Rehan Chaudhry http://orcid.org/0000-0002-3122-8740
Adnan Daud Khan http://orcid.org/0000-0002-6579-4564

References

Azeem F. 2015. All optical switching in silicon microspheres [master's thesis]. Fen Bilimleri Enstitüsü, Koç Üniversitesi.

Azeem F. 2022. Active and passive crystalline whispering gallery mode resonators [dissertation]. University of Otago.

Azeem F, Trainor LS, Devane PA, Norman DS, Rueda A, Lambert NJ, Kumari M, Foreman MR, Schwefel HGL. 2021. Dielectric perturbations: anomalous resonance frequency shifts in optical resonators. Optics Letters. 46(10):2477–2480. doi: 10.1364/OL.420791.

Azeem F, Trainor LS, Gao A, Isarov M, Strekalov DV, Schwefel HGL. 2022a. Ultra-low threshold titanium-doped sapphire whispering-gallery laser. Advanced Optical Materials. 10(8):2102137. doi: 10.1002/adom.v10.8.

Azeem F, Trainor LS, Gao A, Isarov M, Strekalov DV, Schwefel HGL. 2022b. Whispering gallery mode resonators: an alternate platform for Ti: sapphire lasers and amplifiers. In: 2022 International Conference on Emerging Trends in Electrical, Control, and Telecommunication Engineering (ETECTE). Lahore: IEEE; p. 1–6.

Ballard Z, Baaske M, Vollmer F. 2015. Stand-off biodetection with free-space coupled asymmetric microsphere cavities. Sensors. 15(4):8968–8980. doi: 10.3390/s150408968.

Barrios CA, Lipson M. 2006. Silicon photonic read-only memory. Journal of Lightwave Technology. 24(7):2898. doi: 10.1109/JLT.2006.875964.

Beltaos A, Meldrum A. 2007. Whispering gallery modes in silicon-nanocrystal-coated silica microspheres. Journal of Luminescence. 126(2):607–613. doi: 10.1016/j.jlumin.2006.10.005.

Bianucci P, Rodríguez J, Clements C, Hessel C, Veinot J, Meldrum A. 2009. Whispering gallery modes in silicon nanocrystal coated microcavities. Physica Status Solidi (a). 206(5):973–975. doi: 10.1002/pssa.v206:5.

Bourhill J, Goryachev M, Creedon D, Johnson BC, Jamieson DN, Tobar ME. 2019. Low-temperature properties of whispering-gallery modes in isotopically pure silicon-28. Physical Review Applied. 11(4):044044. doi: 10.1103/PhysRevApplied.11.044044.

Braginsky V, Gorodetsky M, Ilchenko V. 1989. Quality-factor and nonlinear properties of optical whispering-gallery modes. Physics Letters A. 137(7–8):393–397. doi: 10.1016/0375-9601(89)90912-2.

Breunig I. 2016. Three-wave mixing in whispering gallery resonators. Laser & Photonics Reviews. 10(4):569–587. doi: 10.1002/lpor.v10.4.

Bruel M. 1995. Silicon on insulator material technology. Electronics Letters. 31(14):1201–1202. doi: 10.1049/el:19950805.

Cai L, Pan J, Hu S. 2020. Overview of the coupling methods used in whispering gallery mode resonator systems for sensing. Optics and Lasers in Engineering. 127:105968. doi: 10.1016/j.optlaseng.2019.105968.

Chantada L, Nikolaev N, Ivanov A, Borri P, Langbein W. 2008. Optical resonances in microcylinders: response to perturbations for biosensing. JOSA B. 25(8):1312–1321. doi: 10.1364/JOSAB.25.001312.

Chaudhry MR, Zakwan M, Onbasli MC, Serpenguzel A. 2020. Symmetric meandering distributed feedback structures for silicon photonic circuits. IEEE Journal of Selected Topics in Quantum Electronics. 26(2):1–5. doi: 10.1109/JSTQE.2944.

Chen R, Ta VD, Sun H. 2014. Bending-induced bidirectional tuning of whispering gallery mode lasing from flexible polymer fibers. ACS Photonics. 1(1):11–16. doi: 10.1021/ph400084s.

Chiasera A, Dumeige Y, Feron P, Ferrari M, Jestin Y, Nunzi Conti G, Pelli S, Soria S, Righini GC. 2010. Spherical whispering-gallery-mode microresonators. Laser & Photonics Reviews. 4(3):457–482. doi: 10.1002/lpor.v4:3.

Christensen JT, Azeem F, Trainor LS, Strekalov DV, Schwefel HG. 2022. Distance calibration via newton's rings in yttrium lithium fluoride whispering gallery mode resonators. Optics Letters. 47(23):6053–6056. doi: 10.1364/OL.474539.

Chýlek P. 1990. Resonance structure of Mie scattering: distance between resonances. Journal of the Optical Society of America A. 7(9):1609. doi: 10.1364/JOSAA.7.001609.

Conti GN, Berneschi S, Cosi F, Pelli S, Soria S, Righini G, Merrer PH, Dispenza M, Secchi A. 2011. Coupling of angle polished waveguides to high-Q whispering gallery mode resonators. In: The European Conference on Lasers and Electro-Optics. Munich: Optical Society of America; p. CK_P9.

Farnesi D, Pelli S, Soria S, Conti GN, Le Roux X, Ballester MM, Vivien L, Cheben P, Alonso-Ramos C. 2021. Metamaterial engineered silicon photonic coupler for whispering gallery mode microsphere and disk resonators. Optica. 8(12):1511–1514. doi: 10.1364/OPTICA.438395.

Fernandez-Gonzalvo X, Chen YH, Yin C, Rogge S, Longdell JJ. 2015. Coherent frequency up-conversion of microwaves to the optical telecommunications band in an Er: YSO crystal. Physical Review A. 92(6):062313. doi: 10.1103/PhysRevA.92.062313.

Foreman MR, Sedlmeir F, Schwefel HGL, Leuchs G. 2016. Dielectric tuning and coupling of whispering gallery modes using an anisotropic prism. Journal of the Optical Society of America B. 33 (11):2177. doi: 10.1364/JOSAB.33.002177.

Frey BJ, Leviton DB, Madison TJ. 2006. Temperature-dependent refractive index of silicon and germanium. In: Optomechanical technologies for astronomy, edited by E. Atad-Ettedgui, J. Antebi, D. Lemke; Vol. 6273. Orlando, FL: SPIE; p. 790–799.

Gandhi R, Leonhardt R, Vogt DW. 2021. Microresonator frequency reference for terahertz precision sensing and metrology. IEEE Transactions on Terahertz Science and Technology. 12 (1):70–74. doi: 10.1109/TTHZ.2021.3119964.

Garrett C, Kaiser W, Bond W. 1961. Stimulated emission into optical whispering modes of spheres. Physical Review. 124(6):1807. doi: 10.1103/PhysRev.124.1807.

Ghulinyan M, Navarro-Urrios D, Pitanti A, Lui A, Pucker G, Pavesi L. 2008. Whispering-gallery modes and light emission from a si-nanocrystal-based single microdisk resonator. Optics Express. 16(17):13218–13224. doi: 10.1364/OE.16.013218.

Gorodetsky ML, Savchenkov AA, Ilchenko VS. 1996. Ultimate Q of optical microsphere resonators. Optics Letters. 21(7):453–455. doi: 10.1364/OL.21.000453.

He C, Sun H, Mo J, Yang C, Feng G, Zhou H, Zhou S. 2018. Temperature sensor based on high-Q polymethylmethacrylate optical microbubble. Laser Physics. 28(7):076202. doi: 10.1088/1555-6611/aab452.

Hendry I, Trainor LS, Xu Y, Coen S, Murdoch SG, Schwefel HGL, Erkintalo M. 2020. Experimental observation of internally pumped parametric oscillation and quadratic comb generation in a $\chi^{(2)}$ whispering-gallery-mode microresonator. Optics Letters. 45(5):1204–1207. doi: 10.1364/OL.385751.

Humayun MH, Khan I, Azeem F, Chaudhry MR, Gökay US, Murib MS, Serpengüzel A. 2018. Far-infrared elastic scattering proposal for the Avogadro Project's silicon spheres. Journal of Quantitative Spectroscopy and Radiative Transfer. 210:173–179. doi: 10.1016/j.jqsrt.2017.12.023.

Ilchenko V, Volikov P, Velichansky V, Treussart F, Lefèvre-Seguin V, Raimond JM, Haroche S. 1998. Strain-tunable high-Q optical microsphere resonator. Optics Communications. 145(1–6):86–90. doi: 10.1016/S0030-4018(97)00439-2.

Ioppolo T, Ötügen MV. 2007. Pressure tuning of whispering gallery mode resonators. Journal of the Optical Society of America B. 24(10):2721. doi: 10.1364/JOSAB.24.002721.

Kim K, Yoon S, Seo M, Lee S, Cho H, Meyyappan M, Baek CK. 2019. Whispering gallery modes enhance the near-infrared photoresponse of hourglass-shaped silicon nanowire photodiodes. Nature Electronics. 2(12):572–579. doi: 10.1038/s41928-019-0317-z.

Kippenberg T, Spillane S, Vahala K. 2004. Kerr-nonlinearity optical parametric oscillation in an ultrahigh-Q toroid microcavity. Physical Review Letters. 93(8):083904. doi: 10.1103/PhysRevLett.93.083904.

Kippenberg TJA. 2004. Nonlinear optics in ultra-high-Q whispering-gallery optical microcavities. California Institute of Technology.

Koehler L, Chevalier P, Shim E, Desiatov B, Shams-Ansari A, Piccardo M, Okawachi Y, Yu M, Loncar M, Lipson M, et al. 2018. Direct thermo-optical tuning of silicon microresonators for the mid-infrared. Optics Express. 26(26):34965–34976. doi: 10.1364/OE.26.034965.

Komma J, Schwarz C, Hofmann G, Heinert D, Nawrodt R. 2012. Thermo-optic coefficient of silicon at 1550 nm and cryogenic temperatures. Applied Physics Letters. 101(4):041905. doi: 10.1063/1.4738989.

Kumar RR, Wang Y, Zhang Y, Tsang HK. 2020. Quantum states of higher-order whispering gallery modes in a silicon micro-disk resonator. JOSA B. 37(8):2231–2237. doi: 10.1364/JOSAB.385551.

Lam C, Leung PT, Young K. 1992. Explicit asymptotic formulas for the positions, widths, and strengths of resonances in Mie scattering. JOSA B. 9(9):1585–1592. doi: 10.1364/JOSAB.9.001585.

Lambert NJ, Trainor LS, Schwefel HGL. 2023. Microresonator-based electro-optic dual frequency comb. Communications Physics. 6(1):89. doi: 10.1038/s42005-023-01197-x.

Li H. 1980. Refractive index of silicon and germanium and its wavelength and temperature derivatives. Journal of Physical and Chemical Reference Data. 9(3):561–658. doi: 10.1063/1.555624.

Lin J, Farajollahi S, Fang Z, Yao N, Gao R, Guan J, Deng L, Lu T, Wang M, Zhang H, et al. 2022. Electro-optic tuning of a single-frequency ultranarrow linewidth microdisk laser. Advanced Photonics. 4(3):036001–036001. doi: 10.1117/1.AP.4.3.036001.

Liu D, Xu H, Tan Y, Shi Y, Dai D. 2021. Silicon photonic filters. Microwave and Optical Technology Letters. 63(9):2252–2268. doi: 10.1002/mop.v63.9.

Lorenz L. 1890. Lysbevaege i og uder en plane lysbolger belyst kulge. Vidensk Selk Skr. 6:1–62.

Ma L, Trainor LS, King GG, Schwefel HGL, Longdell JJ. 2023. Optically detected magnetic resonance to characterize atomlike microwave-optical transducers. Physical Review A. 107(5):053514. doi: 10.1103/PhysRevA.107.053514.

Mack CA. 2011. Fifty years of Moore's law. IEEE Transactions on Semiconductor Manufacturing. 24(2):202–207. doi: 10.1109/TSM.2010.2096437.

Maleki L, Ilchenko VS, Savchenkov AA, Matsko AB. 2009. Crystalline whispering gallery mode resonators in optics and photonics. In: Practical applications of microresonators in optics and photonics, edited by A. B. Matsko. Boca Raton: CRC Press; p. 133–209. doi: 10.1201/9781315218960.

Masini G, Colace L, Assanto G. 2002. Si based optoelectronics for communications. Materials Science and Engineering: B. 89(1-3):2–9. doi: 10.1016/S0921-5107(01)00781-4.

Matsko AB, Ilchenko VS. 2006. Optical resonators with whispering-gallery modes-part I: basics. IEEE Journal of Selected Topics in Quantum Electronics. 12(1):3–14. doi: 10.1109/JSTQE.2005.862952.

McAuslan D, Korystov D, Longdell J. 2011. Coherent spectroscopy of rare-earth-metal-ion-doped whispering-gallery-mode resonators. Physical Review A. 83(6):063847. doi: 10.1103/PhysRevA.83.063847.

McAuslan D, Longdell JJ, Sellars M. 2009. Strong-coupling cavity QED using rare-earth-metal-ion dopants in monolithic resonators: what you can do with a weak oscillator. Physical Review A. 80(6):062307. doi: 10.1103/PhysRevA.80.062307.

Mie G. 1908. Beiträge zur Optik trüber Medien, speziell kolloidaler Metallösungen. Annalen der Physik. 330(3):377–445. doi: 10.1002/andp.v330:3.

Ng V, Azeem F, Trainor LS, Schwefel HGL, Coen S, Erkintalo M, Murdoch SG. 2023. Wideband multimode optical parametric oscillation in a kerr microresonator. Optics Express. 31(4):5475–5482. doi: 10.1364/OE.480030.

Norman DS, Azeem F, Longdell JJ, Schwefel HGL. 2022. Measuring optical loss in yttrium orthosilicate using a whispering gallery mode resonator. Materials for Quantum Technology. 2(1):011001. doi: 10.1088/2633-4356/ac4c39.

Okada Y, Tokumaru Y. 1984. Precise determination of lattice parameter and thermal expansion coefficient of silicon between 300 and 1500 k. Journal of Applied Physics. 56(2):314–320. doi: 10.1063/1.333965.

Oxborrow M. 2007. Traceable 2-d finite-element simulation of the whispering-gallery modes of axisymmetric electromagnetic resonators. IEEE Transactions on Microwave Theory and Techniques. 55(6):1209–1218. doi: 10.1109/TMTT.2007.897850.

Platt LM, Suresh MI, Azeem F, Trainor LS, Schwefel HGL. 2024. Single-point-diamond-turned GaAs disk resonator with over a million optical quality factor. Available from: 10.1364/opticaopen.26519128.v1

Prabhu SS, Achanta VG. 2020. Whispering gallery modes at THz. Advanced Optical Materials. 8(3):1900973. doi: 10.1002/adom.v8.3.

Price MB, Lewellen K, Hardy J, Lockwood SM, Zemke-Smith C, Wagner I, Gao M, Grand J, Chen K, Hodgkiss JM, et al. 2020. Whispering-gallery mode lasing in perovskite nanocrystals chemically bound to silicon dioxide microspheres. The Journal of Physical Chemistry Letters. 11 (17):7009–7014. doi: 10.1021/acs.jpclett.0c02003.

Qian SX, Snow JB, Tzeng HM, Chang RK. 1986. Lasing droplets: highlighting the liquid-air interface by laser emission. Science. 231(4737):486–488. doi: 10.1126/science.231.4737.486.

Qureshi PC, Ng V, Azeem F, Trainor LS, Schwefel HGL, Coen S, Erkintalo M, Murdoch SG. 2022. Soliton linear-wave scattering in a kerr microresonator. Communications Physics. 5(1):123. doi: 10.1038/s42005-022-00903-5.

Ramiro-Manzano F, Prtljaga N, Pavesi L, Pucker G, Ghulinyan M. 2012. A fully integrated high-Q whispering-gallery wedge resonator. Optics Express. 20(20):22934–22942. doi: 10.1364/OE.20.022934.

Ramiro-Manzano F, Prtljaga N, Pavesi L, Pucker G, Ghulinyan M. 2013. Thermo-optical bistability with Si nanocrystals in a whispering gallery mode resonator. Optics Letters. 38(18):3562–3565. doi: 10.1364/OL.38.003562.

Rayleigh L. 1878. Theory of sound. Vol. 2. London: MacMillan and Co; p. 115.

Rayleigh L. 1910. CXII. *The problem of the whispering gallery*. The London, Edinburgh, and Dublin Philosophical Magazine and Journal of Science. 20(120):1001–1004. doi: 10.1080/14786441008636993.

Rayleigh L. 1912. The Scientific Papers of Lord Rayleigh. Vols (1-4). New York: Cambridge University Press.

Rayleigh L. 1914. IX. *Further applications of Bessel's functions of high order to the Whispering Gallery and allied problems*. The London, Edinburgh, and Dublin Philosophical Magazine and Journal of Science. 27(157):100–109. doi: 10.1080/14786440108635067.

Reynolds T, Riesen N, Meldrum A, Fan X, Hall JM, Monro TM, François A. 2017. Fluorescent and lasing whispering gallery mode microresonators for sensing applications. Laser & Photonics Reviews. 11(2):1600265. doi: 10.1002/lpor.v11.2.

Richtmyer R. 1939. Dielectric resonators. Journal of Applied Physics. 10(6):391–398. doi: 10.1063/1.1707320.

Righini GC, Dumeige Y, Feron P, Ferrari M, Conti GN, Ristic D, Soria S. 2011. Whispering gallery mode microresonators: fundamentals and applications. Riv Nuovo Cimento. 34(7):435–488. doi: 10.1393/ncr/i2011-10067-2.

Rodriguez J, Veinot J, Bianucci P, Meldrum A. 2008. Whispering gallery modes in hollow cylindrical microcavities containing silicon nanocrystals. Applied Physics Letters. 92(13):131119. doi: 10.1063/1.2903134.

Roselló-Mechó X, Farnesi D, Frigenti G, Barucci A, Fernández-Bienes A, García-Fernández T, Ratto F, Delgado-Pinar M, Andrés MV, Nunzi Conti G, et al. 2019. Parametrical optomechanical oscillations in phoxonic whispering gallery mode resonators. Scientific Reports. 9(1):1–7. doi: 10.1038/s41598-018-37186-2.

Rueda A, Sedlmeir F, Collodo MC, Vogl U, Stiller B, Schunk G, Strekalov DV, Marquardt C, Fink JM, Painter O, et al. 2016. Efficient microwave to optical photon conversion: an electro-optical realization. Optica. 3(6):597–604. doi: 10.1364/OPTICA.3.000597.

Rueda A, Sedlmeir F, Kumari M, Leuchs G, Schwefel HGL. 2019. Resonant electro-optic frequency comb. Nature. 568(7752):378–381. doi: 10.1038/s41586-019-1110-x.

Sadrozinski HW, Ely S, Fadeyev V, Galloway Z, Ngo J, Parker C, Petersen B, Seiden A, Zatserklyaniy A, Cartiglia N, et al. 2013. Ultra-fast silicon detectors. Nuclear Instruments and Methods in Physics Research Section A: Accelerators, Spectrometers, Detectors and Associated Equipment. 730:226–231. doi: 10.1016/j.nima.2013.06.033.

Savchenkov A, Ilchenko V, Matsko A, Maleki L. 2003. Tunable filter based on whispering gallery modes. Electronics Letters. 39(4):389. doi: 10.1049/el:20030229.
Savchenkov AA, Matsko AB, Ilchenko VS, Maleki L. 2007. Optical resonators with ten million finesse. Optics Express. 15(11):6768–6773. doi: 10.1364/OE.15.006768.
Sayson NLB, Bi T, Ng V, Pham H, Trainor LS, Schwefel HGL, Coen S, Erkintalo M, Murdoch SG. 2019. Octave-spanning tunable parametric oscillation in crystalline kerr microresonators. Nature Photonics. 13(10):701–706. doi: 10.1038/s41566-019-0485-4.
Sayson NLB, Pham H, Webb KE, Ng V, Trainor LS, Schwefel HGL, Coen S, Erkintalo M, Murdoch SG. 2018. Origins of clustered frequency combs in kerr microresonators. Optics Letters. 43 (17):4180–4183. doi: 10.1364/OL.43.004180.
Sedlmeir F. 2016. Crystalline whispering gallery mode resonators [dissertation]. Friedrich-Alexander-Universität Erlangen-Nürnberg (FAU).
Seo M, Kim K, Cho H, Yoon S, Kong BD, Meyyappan M, Baek CK. 2019. Weakly tapered silicon nanopillar resonators with spatially well-separated whispering gallery modes for Si-based lasers. ACS Applied Nano Materials. 2(8):4852–4858. doi: 10.1021/acsanm.9b00810.
Shitikov A, Bilenko I, Kondratiev N, Lobanov V, Markosyan A, Gorodetsky M. 2018. Billion Q-factor in silicon WGM resonators. Optica. 5(12):1525–1528. doi: 10.1364/OPTICA.5.001525.
Smirnov AY, Rashkeev S, Zagoskin A. 2002. Polarization switching in optical microsphere resonator. Applied Physics Letters. 80(19):3503–3505. doi: 10.1063/1.1477277.
Soltani M, Ilchenko V, Matsko A, Savchenkov A, Schlafer J, Ryan C, Maleki L. 2016. Ultrahigh Q whispering gallery mode electro-optic resonators on a silicon photonic chip. Optics Letters. 41 (18):4375–4378. doi: 10.1364/OL.41.004375.
Soref R, Lorenzo J. 1985. Single-crystal silicon: a new material for 1.3 and 1.6 μm integrated-optical components. Electronics Letters. 21(21):953–954. doi: 10.1049/el:19850673.
Stratton JA. 2007. Electromagnetic theory. Vol. 33. Hoboken, NJ: John Wiley & Sons, Inc.
Strekalov D, Thompson R, Baumgartel L, Grudinin I, Yu N. 2011. Temperature measurement and stabilization in a birefringent whispering gallery mode resonator. Optics Express. 19(15):14495–14501. doi: 10.1364/OE.19.014495.
Strekalov DV, Marquardt C, Matsko AB, Schwefel HGL, Leuchs G. 2016. Nonlinear and quantum optics with whispering gallery resonators. Journal of Optics. 18(12):123002 doi: 10.1088/2040-8978/18/12/123002.[accessed 2019 May 27]. Available from: http://stacks.iop.org/2040-8986/18/i=12/a=123002?key=crossref.81a05321becb6affdf43a13d82aeaa5a.
Su Y, Zhang Y, Qiu C, Guo X, Sun L. 2020. Silicon photonic platform for passive waveguide devices: materials, fabrication, and applications. Advanced Materials Technologies. 5 (8):1901153. doi: 10.1002/admt.v5.8.
Su Z, Hosseini ES, Timurdogan E, Sun J, Moresco M, Leake G, Adam TN, Coolbaugh DD, Watts MR. 2017. Whispering gallery germanium-on-silicon photodetector. Optics Letters. 42 (15):2878–2881. doi: 10.1364/OL.42.002878.
Subramanian S, Jones HB, Frustaci S, Winter S, van der Kamp MW, Arcus VL, Pudney CR, Vollmer F. 2021. Sensing enzyme activation heat capacity at the single-molecule level using gold-nanorod-based optical whispering gallery modes. ACS Applied Nano Materials. 4 (5):4576–4583. doi: 10.1021/acsanm.1c00176.
Suresh MI, Schwefel HGL, Vogt DW. 2023. Gallium arsenide whispering gallery mode resonators for terahertz photonics. Optics Express. 31(20):33056–33063. doi: 10.1364/OE.498406.
Tapalian C, Laine JP, Lane P. 2001. Thermo-optical switches using coated microsphere resonators. MRS Online Proceedings Library (OPL). 694:K3.9.1–K3.9.6.
Tewary A, Digonnet MJF, Sung JY, Shin JH, Brongersma ML. 2006. Silicon-nanocrystal-coated silica microsphere thermooptical switch. IEEE Journal of Selected Topics in Quantum Electronics. 12(6):1476–1479. doi: 10.1109/JSTQE.2006.885389.
Trainor LS. 2021. Optical parametric frequency generation in whispering-gallery resonators [dissertation]. Department of Physics, University of Otago.
Trainor LS, Sedlmeir F, Peuntinger C, Schwefel HGL. 2018. Selective coupling enhances harmonic generation of whispering-gallery modes. Physical Review Applied. 9(2):024007. doi: 10.1103/PhysRevApplied.9.024007.

Vogt DW. 2022. Terahertz microresonators for material characterisation. Optical Materials Express. 12(9):3463–3470. doi: 10.1364/OME.461273.
Vogt DW, Jones AH, Leonhardt R. 2018. Thermal tuning of silicon terahertz whispering-gallery mode resonators. Applied Physics Letters. 113(1):011101. doi: 10.1063/1.5036539.
Vogt DW, Jones AH, Leonhardt R. 2020. Terahertz gas-phase spectroscopy using a sub-wavelength thick ultrahigh-Q microresonator. Sensors. 20(10):3005. doi: 10.3390/s20103005.
Vogt DW, Jones AH, Schwefel HGL, Leonhardt R. 2019. Anomalous blue-shift of terahertz whispering-gallery modes via dielectric and metallic tuning. Optics Letters. 44(6):1319–1322. doi: 10.1364/OL.44.001319.
Vogt DW, Leonhardt R. 2018. Ultra-high Q terahertz whispering-gallery modes in a silicon resonator. APL Photonics. 3(5):051702-1–051702-9. doi: 10.1063/1.5010364.
von Klitzing W, Jahier E, Long R, Lissillour F, Lefèvre-Seguin V, Hare J, Raimond JM, Haroche S. 2000. Very low threshold green lasing in microspheres by up-conversion of IR photons. Journal of Optics B: Quantum and Semiclassical Optics. 2(2):204–206. doi: 10.1088/1464-4266/2/2/324.
Ward JM, Chormaic SN. 2010. Thermo-optical tuning of whispering gallery modes in Er:Yb co-doped phosphate glass microspheres. Applied Physics B. 100(4):847–850. doi: 10.1007/s00340-010-4153-0.
Watanabe H, Yamada N, Okaji M. 2004. Linear thermal expansion coefficient of silicon from 293 to 1000 k. International Journal of Thermophysics. 25(1):221–236. doi: 10.1023/B:IJOT.0000022336.83719.43.
Werner CS, Sturman B, Podivilov E, Manjeshwar SK, Buse K, Breunig I. 2018. Control of mode anticrossings in whispering gallery microresonators. Optics Express. 26(2):762–771. doi: 10.1364/OE.26.000762.
Witzens J. 2018. High-speed silicon photonics modulators. Proceedings of the IEEE. 106 (12):2158–2182. doi: 10.1109/JPROC.2018.2877636.
Yilmaz Y, Demir A, Kurt A, Serpenguzel A. 2005. Optical channel dropping with a silicon microsphere. IEEE Photonics Technology Letters. 17(8):1662–1664. doi: 10.1109/LPT.2005.850896.
Zhu J, Özdemir ŞK, Yilmaz H, Peng B, Dong M, Tomes M, Carmon T, Yang L. 2014. Interfacing whispering-gallery microresonators and free space light with cavity enhanced Rayleigh scattering. Scientific Reports. 4:6396. doi: 10.1038/srep06396.